Cardiovascular Research (2015) **107**, 175–183
doi:10.1093/cvr/cvv149

Stochastic spontaneous calcium release events trigger premature ventricular complexes by overcoming electrotonic load

Fernando O. Campos[1], Yohannes Shiferaw[2], Anton J. Prassl[1], Patrick M. Boyle[3], Edward J. Vigmond[4,5], and Gernot Plank[1]*

[1]Institute of Biophysics, Medical University of Graz, Graz, Austria; [2]Department of Physics, California State University, Northridge, CA, USA; [3]Institute for Computational Medicine, Johns Hopkins University, Baltimore, MD, USA; [4]LIRYC Institute, University of Bordeaux, Bordeaux, France; and [5]Department of Electrical and Computer Engineering, University of Calgary, Calgary, Canada

Received 29 October 2014; revised 15 April 2015; accepted 7 May 2015; online publish-ahead-of-print 12 May 2015

Time for primary review: 39 days

Aims Premature ventricular complexes (PVCs) due to spontaneous calcium (Ca) release (SCR) events at the cell level can precipitate ventricular arrhythmias. However, the mechanistic link between SCRs and PVC formation remains incompletely understood. The aim of this study was to investigate the conditions under which delayed afterdepolarizations resulting from stochastic subcellular SCR events can overcome electrotonic source–sink mismatch, leading to PVC initiation.

Methods and results A stochastic subcellular-scale mathematical model of SCR was incorporated in a realistic model of the rabbit ventricles and Purkinje system (PS). Elevated levels of diastolic sarcoplasmic reticulum Ca^{2+} (Ca_{SR}) were imposed until triggered activity was observed, allowing us to compile statistics on probability, timing, and location of PVCs. At $Ca_{SR} \geq 1500$ μmol/L PVCs originated in the PS. When SCR was incapacitated in the PS, PVCs also emerged in the ventricles, but at a higher Ca_{SR} ($\geq$1550 μmol/L) and with longer waiting times. For each model configuration tested, the probability of PVC occurrence increased from 0 to 100% within a well-defined critical Ca_{SR} range; this transition was much more abrupt in organ-scale models (~50 μmol/L Ca_{SR} range) than in the tissue strand (~100 μmol/L) or single-cell (~450 μmol/L) models. Among PVCs originating in the PS, ~68% were located near Purkinje-ventricular junctions (<1 mm).

Conclusion SCR events overcome source–sink mismatch to trigger PVCs at a critical Ca_{SR} threshold. Above this threshold, PVCs emerge due to increased probability and reduced variability in timing of SCR events, leading to significant diastolic depolarization. Sites of lower electronic load, such as the PS, are preferential locations for triggering.

Keywords Delayed afterdepolarization • Triggered activity • Computer-based model • Purkinje system • Arrhythmia

1. Introduction

Arrhythmias are the leading cause of sudden death in patients with cardiac diseases such as myocardial ischaemia or heart failure (HF).[1,2] Ectopic excitations are believed to be implicated in triggering a variety of these arrhythmias by causing premature ventricular complexes (PVCs). These are usually benign in healthy individuals[3]; however, under diseased conditions they can disrupt the normal sinus rhythm and precipitate life-threatening tachycardias.[4,5]

Ectopic excitations have been the topic of many experimental studies ranging from cellular to whole heart preparations.[6–11] At the cellular level, they can occur when action potentials (APs) are elicited by suprathreshold afterdepolarizations caused by abnormalities at the level of ion channels. Afterdepolarizations occur either early during the plateau phase of a long-duration AP or 'delayed', when the AP is nearly or fully repolarized. With delayed afterdepolarizations (DADs), it is well established that abnormal calcium (Ca^{2+}) cycling plays an essential role in their genesis.[6,7,9,11,12] Ca^{2+} release from the sarcoplasmic

* Corresponding author. Tel: +43 316 380 7756, Fax: +43 316 380 9660, Email: gernot.plank@medunigraz.at

reticulum (SR) due to random openings of Ryanodine receptors can generate spontaneous Ca^{2+} sparks in absence of any local trigger current provided through L-type Ca^{2+} channel activation.[9] Such spontaneous Ca^{2+} release (SCR) events are favoured by conditions producing Ca^{2+} overload such as ischaemia, increased sympathetic nerve activity, hypertrophy, or HF.[13–15] Spontaneous Ca^{2+} sparks can spread throughout the cell as waves, stimulating Ca^{2+}-sensitive inward currents which can summate to produce a DAD-induced AP.

While such DADs may induce APs in isolated myocytes, this is not necessarily the case in tissue where myocytes are coupled via gap junctions to quiescent neighbouring myocytes. DADs induce electrotonic current flow, which greatly reduces its magnitude compared with isolated myocytes. For triggered APs to propagate, it is necessary that DADs occur within a sufficiently small window in time over a larger ensemble of adjacent myocytes to achieve suprathreshold depolarization. However, the mechanism by which spatiotemporal synchronization of stochastic SCR events is achieved in tissue remains poorly understood.

The objective of this study is to test the hypotheses that (i) a critical diastolic threshold in SR Ca^{2+} load (Ca_{SR}) exists above which PVCs emerge without the need for a mechanism to synchronize stochastic SCRs across cells, and (ii) electrotonic loading conditions in structurally healthy ventricles favour the origin of the first DAD-induced PVC in the Purkinje system (PS). These hypotheses are tested using a phenomenological model of SCR[16] and AP[17] which is incorporated into an anatomically accurate computer model of rabbit ventricles, equipped with a topologically realistic His-Purkinje system.[18] Heterogeneities in cellular electrophysiology in ventricular as well as Purkinje cells are ignored to precisely assess the role of electrotonic load in PVC formation.

2. Methods

2.1 Model of spontaneous Ca^{2+} release and ventricular action potential

In ventricular myocytes, efflux of Ca^{2+} from the SR can occur spontaneously due to Ryanodine receptor (RyR) openings during diastole, independently of Ca^{2+} influx via L-type Ca^{2+} channels. Random RyR openings can induce spontaneous Ca^{2+} sparks, which can propagate to form Ca^{2+} waves, and depolarize the membrane to generate DADs. While computer models have been developed which explicitly account for spatio-temporal features of subcellular Ca^{2+} and stochastic transitions in individual RyRs, these are computationally prohibitive for investigating organ scale DAD formation.[19–21] Thus, in this study, an experimentally based phenomenological model of SCR[16] has been employed and coupled to the Mahajan-Shiferaw (MSH)[17] rabbit ventricular AP model. Stochastic SCR events are represented as Ca^{2+} waves that are nucleated in the cell and then propagate as fire-diffuse-fire waves. Details of Ca^{2+} waves formation as well as their functional dependence on Ca_{SR} are given in the Supplementary material online. To generate DADs, key parameters of the MSH model were modified[22] based on experimental data collected under HF conditions,[23] which are known to increase the propensity for DADs (see Supplementary material online).

2.2 Biventricular model

This DAD-prone myocyte model was incorporated into an anatomically accurate 3D computer model of the rabbit ventricles[18] including a topologically realistic model of the PS. Electrical activity was solved with the CARP simulator[24] using the monodomain approach. The same MSH myocyte model was used in both ventricles and PS to rule out any effects due to electrophysiological heterogeneities. This renders the formation of PVCs a sole function of dimensionality (3D ventricles and quasi-1D PS), biventricular anatomy, anisotropy, and Ca_{SR}.

2.3 Simulation protocol

Similar to experiments,[15,25] myocyte models were paced at 2.5 Hz for 100 cycles to stabilize under varying extracellular Ca^{2+} concentrations, followed by a 1000-ms pause within which DAD formation was recorded. Extracellular Ca^{2+} concentration was increased to induce different diastolic levels of SR Ca^{2+} overload in the range 1000–1600 μmol/L (see Supplementary material online, *Figure S1* and *Table S1*). Due to the stochastic nature of SCR, $N = 1110$ independent single myocyte experiments with different random seeds were performed for each Ca_{SR}. The exact same protocol was applied in the biventricular model, which was paced in space-clamped mode. Each myocyte in the model was assigned a unique random seed to ensure heterogeneous stochastic SCR evolution and preclude any dependency of location and timing of PVC formation on the preceding activation sequence. In the biventricular model, $N = 100$ experiments were performed for each Ca_{SR}.

2.4 Data analysis

For each Ca_{SR}, the number of experiments in which a SCR event with a recruitment rate >5 sparks/ms was observed within the pacing pause, n, was recorded to compute the probability $p_{SCR} = n/N$. This recruitment rate criterion was sufficiently high to be only met if Ca^{2+} waves propagated throughout the whole cell. Given this definition, p_{SCR} is equivalent to the probability of a propagating Ca^{2+} wave to occur in a given time interval within a single-cell. Likewise, p_{AP} is the probability of a cell to trigger an AP during the pacing pause. The number of SCR events as well as the time until the onset of a SCR event, T_{SCR}, and a triggered AP, T_{AP}, were determined (*Figure 1*). Experiments were repeated with the fast sodium current, I_{Na}, and the L-type Ca^{2+} current, I_{CaL}, inhibited, to compute the intrinsic spontaneous Ca^{2+} elevation in the submembrane space, ΔCa_s, and DAD amplitude, ΔV_m, as a sole function of SCR. In tissue experiments, the location of the first PVC was also recorded.

3. Results

3.1 Ca^{2+}-mediated triggered activity in isolated cells

Ca^{2+} and voltage traces during the last three of the 100 pacing cycles are shown in *Figure 1* to illustrate different outcomes of the same stochastic model. In both experiments, SCR events elevated Ca_s, by ΔCa_s, which, in turn, led to a subthreshold (blue trace) depolarization, ΔV_m, or an AP (red trace). *Figure 2* summarizes results obtained for all prescribed Ca_{SR}. Both p_{SCR} and p_{AP} increased in a sigmoid fashion with Ca_{SR} (*Figure 2A*). SCR events occurred over the entire range of Ca_{SR} probed while triggered APs appeared only at $Ca_{SR} \geq 1100$ μmol/L. SCRs or APs always occurred for $Ca_{SR} \geq 1350$ and ≥1450 μmol/L, respectively. This was due to the gradual increase in the number of SCR events, a shortening of T_{SCR}, and a reduced timing variability with increasing Ca_{SR} (*Figure 2B* and *C*). On average, the number of SCR events increased from 715 to 14 340, and average T_{SCR} shortened from 732 to 142 ms, when increasing Ca_{SR} from 1000 to 1600 μmol/L.

Increased incidence of SCR events translated into larger Ca^{2+} elevations and DAD amplitudes. However, at ΔV_m close to or above threshold, the intrinsic contribution of SCR events was masked by the onset of I_{Na} and I_{caL}. To measure the intrinsic driving force, i.e. the dependency of ΔCa_s and ΔV_m on Ca_{SR}, all experiments were repeated with I_{Na} and I_{CaL} currents inhibited. The average of ΔCa_s and ΔV_m increased with Ca_{SR}, but to different extents (*Figure 2D* and *E*). With Ca_{SR}

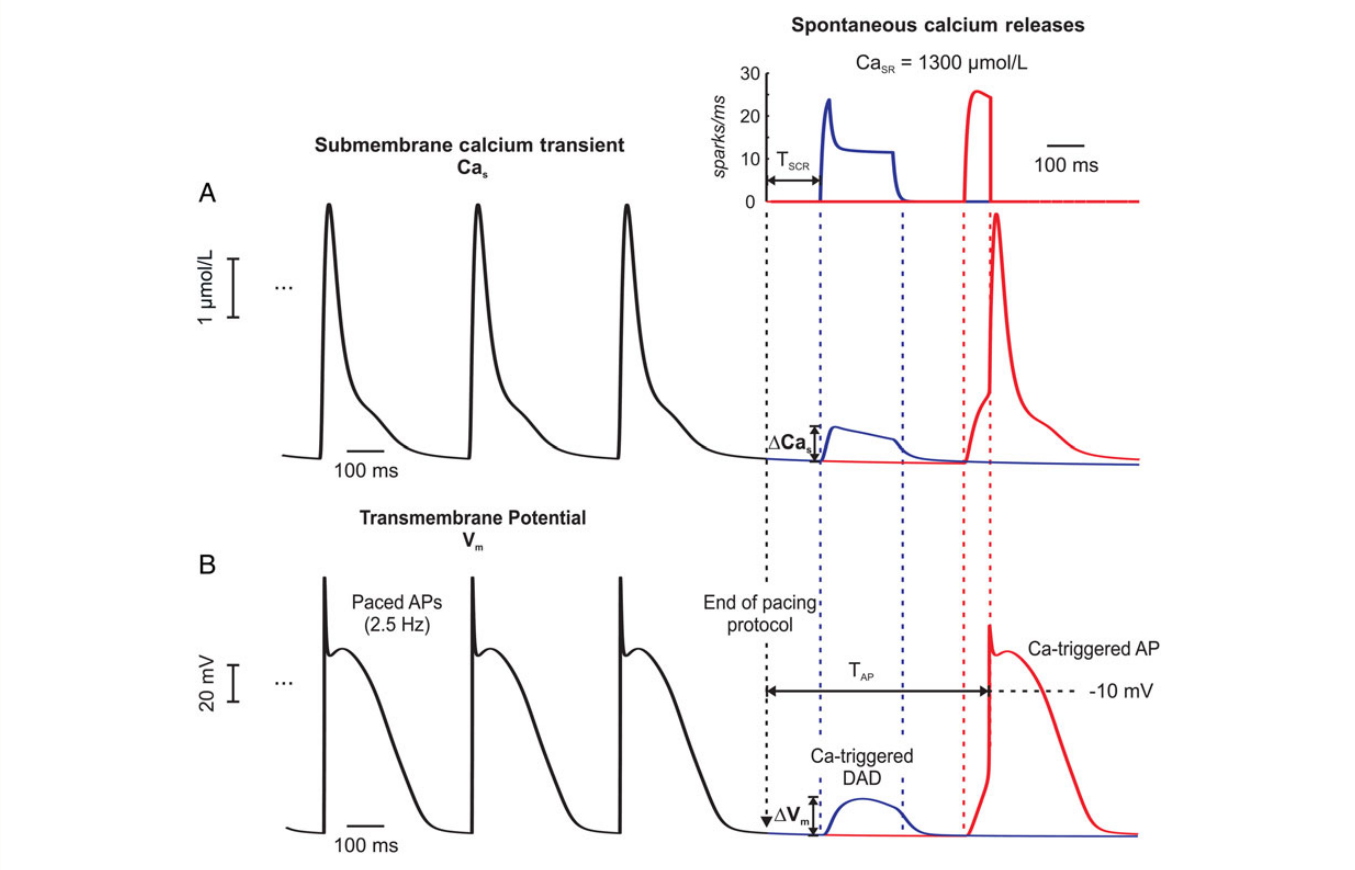

Figure 1 Ca-mediated triggered activity in an isolated myocyte. Shown are Ca_s and V_m traces of the last three out of 100 pacing cycles before a 1000-ms pause. (*A*) Ca^{2+} traces illustrate two different outcomes of the same stochastic model (blue: DAD, red: triggered AP). SCR (inset) led to elevations in the subsarcolemal Ca, ΔCa_s. (*B*) V_m traces taken from the same two experiments in (*A*). The elevations in ΔCa_s induced membrane depolarizations ΔV_m which either turned into a subthreshold DAD (blue trace) or a full-blown AP (red trace).

between 1200 and 1400 µmol/L, corresponding to the rising phase of p_{AP} in *Figure 2A*, statistical variability was large, as reflected in many outliers. These were due to the differences between cells that elicited a triggered AP from those that did not (see differences in p_{SCR} and p_{AP} in *Figure 2A*). The relationship between ΔCa_s and ΔV_m, referred to as 'calcium-membrane voltage coupling gain', was nonlinear, where the average ΔCa_s per Ca_{SR} is plotted against the average ΔV_m (*Figure 2F*).

3.2 Ectopic excitations in a 1D strand of coupled cells

To assess the effect of electrotonic load, all 1110 cells used in single-cell experiments were coupled to form a 1D strand. In this experiment, the same stochastic properties were assigned as previously to the individual cells. This experiment showed that intrinsic properties directly related to SCR events, such as their number, T_{SCR}, and ΔCa_s (data not shown) remained virtually unaffected by coupling; however, noticeable differences were observed in ΔV_m. *Figure 3A* compares ΔV_m of uncoupled and coupled cells for Ca_{SR} ranging from 1400 to 1500 µmol/L. While the average ΔV_m at 1400 µmol/L was much lower in the strand (20 vs. 41 mV), the difference decreased with increasing Ca_{SR}. At Ca_{SR} = 1500 µmol/L, ΔV_m was 32 vs. 43 mV. Further, electrotonic load in the strand smoothed out variability in ΔV_m and decreased calcium-membrane voltage coupling gain (*Figure 3B*). On average, SCR-induced ΔCa_s led to less depolarization; however, the difference attenuated with increasing Ca_{SR}.

The same simulation protocol was used to perform 100 strand experiments (*Figure 3C*). Overall, electrotonic coupling in the strand led to a significant shift in p_{AP} towards higher Ca_{SR} along with a much steeper sigmoid rise around the threshold Ca_{SR}. Ectopic excitations only appeared at a Ca_{SR} of 1450 µmol/L with p_{AP} of 29% and reached 100% at $Ca_{SR} \geq 1500$ µmol/L.

3.3 PVCs in the biventricular model

Compared with the strand experiments, an even steeper transition in p_{AP} from 0 to 100% was observed (*Figure 4A*, orange trace). For $Ca_{SR} \leq$ 1450 µmol/L, no PVCs emerged at all. For $Ca_{SR} \geq 1500$ µmol/L, PVCs emerged in all experiments, indicating a distinct narrow banded threshold zone in Ca_{SR}. Measured T_{AP} were 349 ± 14 ms (1500 µmol/L) and 176 ± 18 ms (1600 µmol/L).

Figure 4B and *C* show the distribution of foci at Ca_{SR} of 1500 and 1600 µmol/L. Despite the much larger number of cells in the ventricles, all foci arose exclusively, without exception, in the PS (see Supplementary material online, *Video S1* for an example). The majority of PVCs (~68%) originated in the distal branches of the PS in the immediate vicinity (<1 mm) of a Purkinje-ventricular junction (PVJ). The

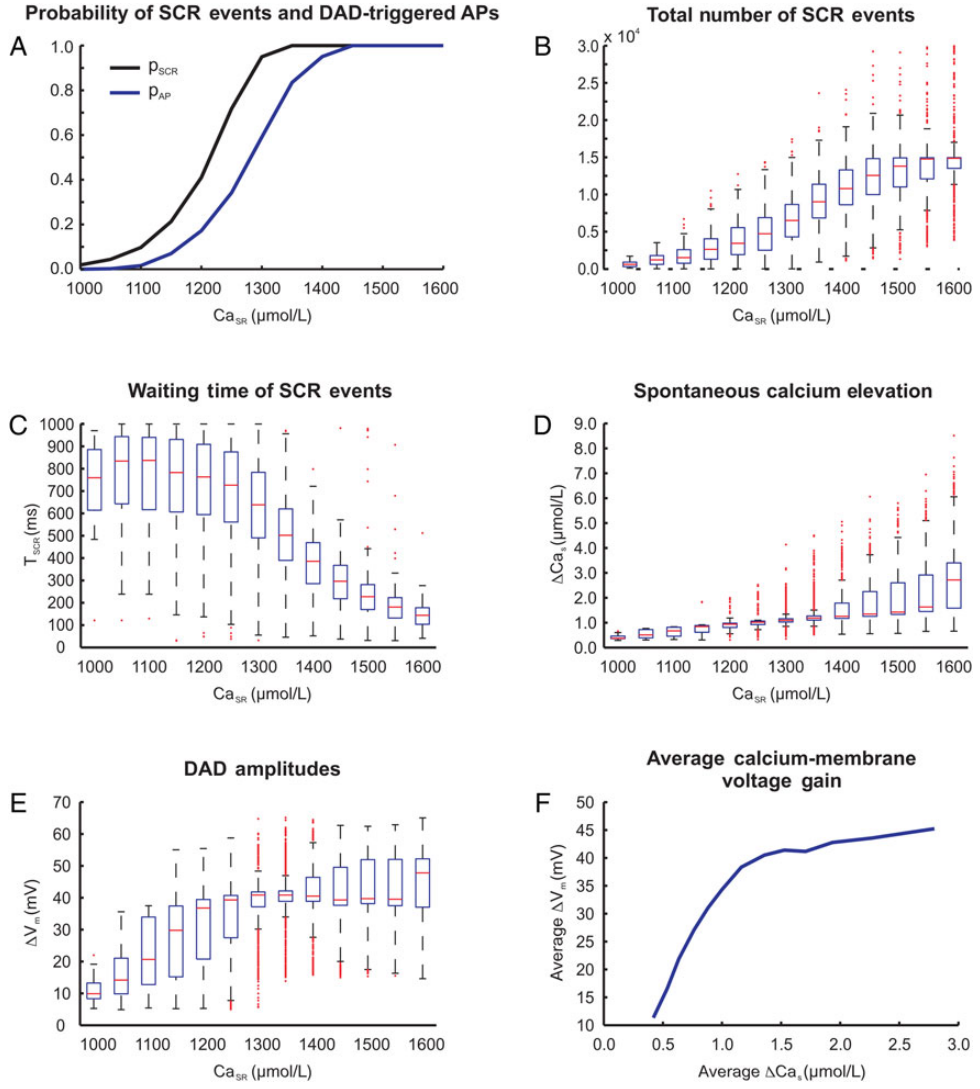

Figure 2 Statistics of triggered activity in $N = 1110$ single-cell experiments at various Ca_{SR}. (*A*) Probability of SCR events p_{SCR} (black trace) and DAD-triggered APs p_{AP} (blue trace). (*B*) Total number of SCR events. (*C*) Waiting time of SCR events, T_{SCR}. (*D*) Spontaneous Ca^{2+} elevation ΔCa_s and (*E*) DAD amplitude ΔV_m due to SCR events. (*F*) Average calcium-membrane voltage gain based on ΔV_m and ΔCa_s averaged over all single-cell experiments.

remaining foci were distributed throughout the PS without any obvious preference.

To establish whether PVCs in the ventricles occurred, but were masked by foci emerging earlier in the PS, experiments were performed where SCR was inhibited in the PS. At a Ca_{SR} of 1500 μmol/L, where p_{AP} was 100% with SCR in the PS enabled, no PVCs occurred (*Figure 4A*, red trace). However, after a minor increase in Ca_{SR} to 1550 μmol/L, PVCs always occurred. Foci were located at either the epicardial or endocardial surface, but none within the depth of the ventricular wall. *Figure 4D* shows the uneven clustering of focal sources along the edges of the base where the source–sink mismatch was less severe.

No major qualitative differences in p_{AP} were found over all experiments from single-cell to ventricles, but quantitatively increased electrotonic load promoted a shift of p_{AP} curves towards higher Ca_{SR} and a steepening of the transition from 0 to 100% probability (*Figure 4A*). The critical threshold in Ca_{SR} necessary for foci to occur with 100% probability was found to be 1450 μmol/L in the single-cell, 1500 μmol/L in the 1D strand and the 3D ventricles with PS, and 1550 μmol/L in the ventricles with SCRs inhibited in the PS.

3.4 PVC mechanism in 3D

In the absence of SCR events in the PS, PVCs in the ventricles appeared for $Ca_{SR} \geq 1550$ μmol/L. The mechanism by which stochastic SCR events achieve sufficient synchronization to trigger a propagated AP is illustrated in *Figures 5* and *6* (see also Supplementary material online, *Video S2*). The stochastic nature of SCR and associated Ca_s is shown in *Figure 5A*. At the focal site, Ca_s started to rise around 90 ms due to a SCR event (*Figure 5B*). Numerous other cells underwent SCRs earlier than this (*Figure 5A*$_2$). At $t_3 = 120$ ms, the instant of maximum rate of rise of spontaneous Ca_s, a Ca_s elevation of 2.2 μmol/L had built up at the focal site which was noticeably larger than the average Ca_s elevation of 1.26 μmol/L in the ventricles (*Figure 5A*$_3$ and *C*). At $t_4 = 156.5$ ms, when the upstroke velocity of the AP peaked, the average Ca_s elevation over the entire ventricles had arrived at 1.93 μmol/L, but numerous

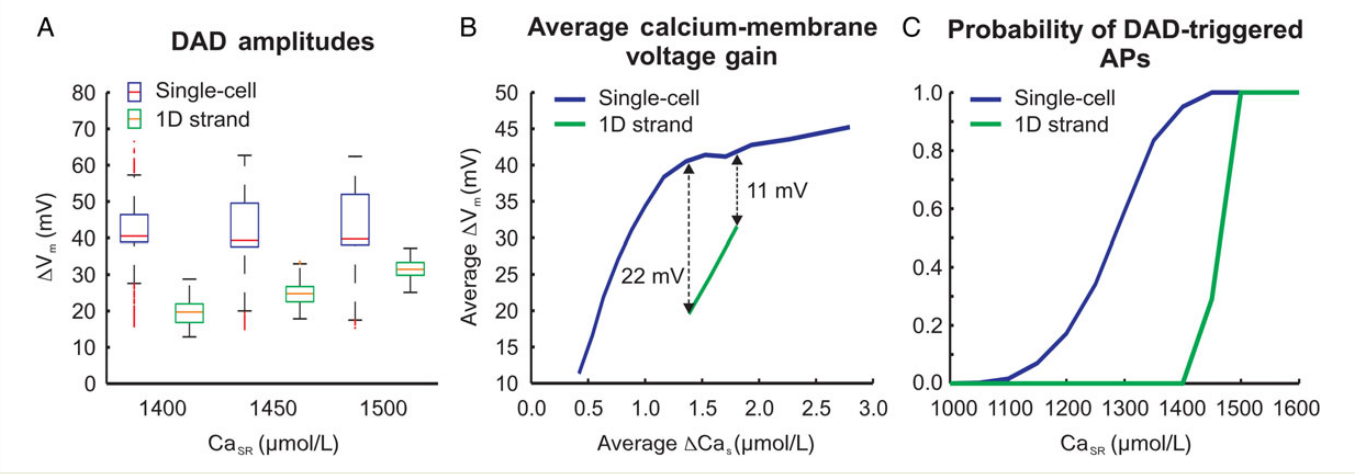

Figure 3 Differences between 1D strand and isolated myocytes. (*A*) ΔV_m due to SCR events. (*B*) Ca-membrane voltage gain: relationship between averaged ΔV_m and averaged ΔCa_s of all single-cell and 1D cable experiments. (*C*) p_{AP} in 1D strand (green trace) relative to isolated myocyte data (blue trace).

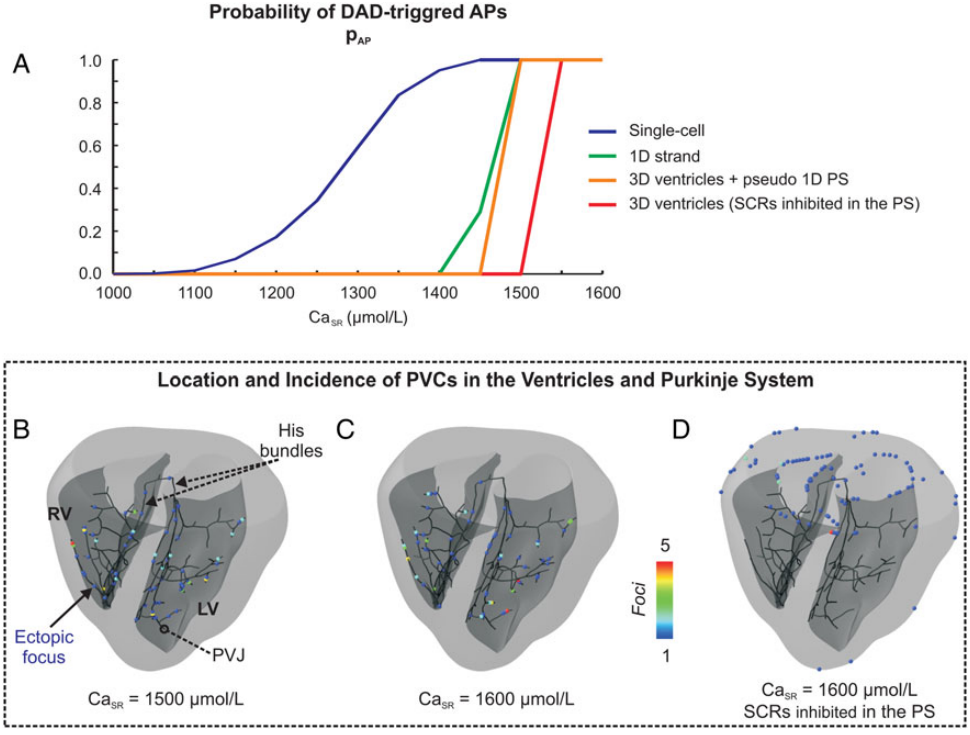

Figure 4 Location and incidence of PVCs in the ventricles and PS. (*A*) p_{AP} under different electrotonic loading conditions. (*B*) Location and incidence of PVCs at a Ca_{SR} of 1500 μmol/L, (*C*) 1600 μmol/L, and (*D*) 1600 μmol/L with SCR inhibited in the PS. Colour coding indicates number of ectopic foci.

sites had higher elevation levels (*Figure 5*A_4 and *C*). The fast increase in Ca_s at t_4 was not solely due to a SCR event, but caused by Ca^{2+} flux via I_{CaL} and Ca^{2+}-induced Ca^{2+} release from the SR.

Membrane depolarization in response to the elevation in Ca_s in the ventricles and at the focal site is shown in *Figure 6A* and *B*, respectively. Note that the PVC did not emerge from a cluster of synchronously firing cells; rather an overall depolarization of the ventricles occurred (Supplemental material online, *Video S2*). At time t_4, when upstroke velocity peaked at the focal site, most cells had undergone significant depolarization (*Figure 6*A_4 and *C*). This was driven by I_{NCX} currents in response to the rise in Ca_s caused by the large number of SCR events, occurring with an average T_{SCR} of 102 ± 58 ms.

4. Discussion

This study used a multiscale computational model of the rabbit ventricles equipped with a topologically realistic model of the PS network to investigate probability, timing, and locations of SCR-mediated PVCs.

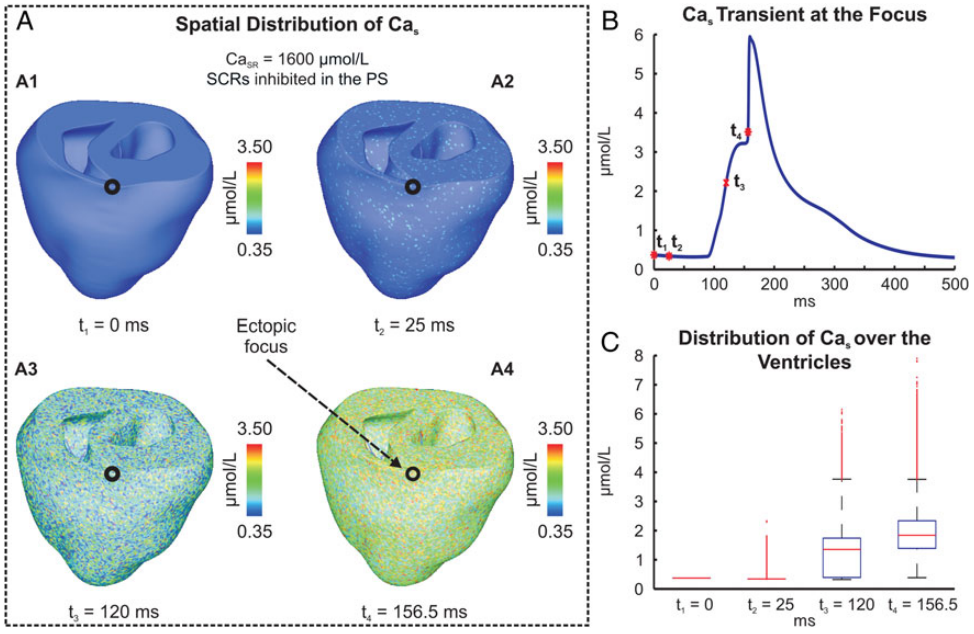

Figure 5 Spontaneous Ca^{2+} elevation and genesis of a PVC in the absence of SCRs in the PS. (*A*) Spatial distribution of Ca_s at time instants: $t_1 = 0$ ms, the start of pacing pause; $t_2 = 25$ ms; $t_3 = 120$ ms, the time of maximum rate of rise of Ca_s at focal site, and $t_4 = 156$ ms, time of maximum rate of rise of the triggered AP. (*B*) Ca_s transient recorded at the ectopic focus. (*C*) Boxplots illustrating distribution of Ca_s over the ventricles at time instants t_1–t_4.

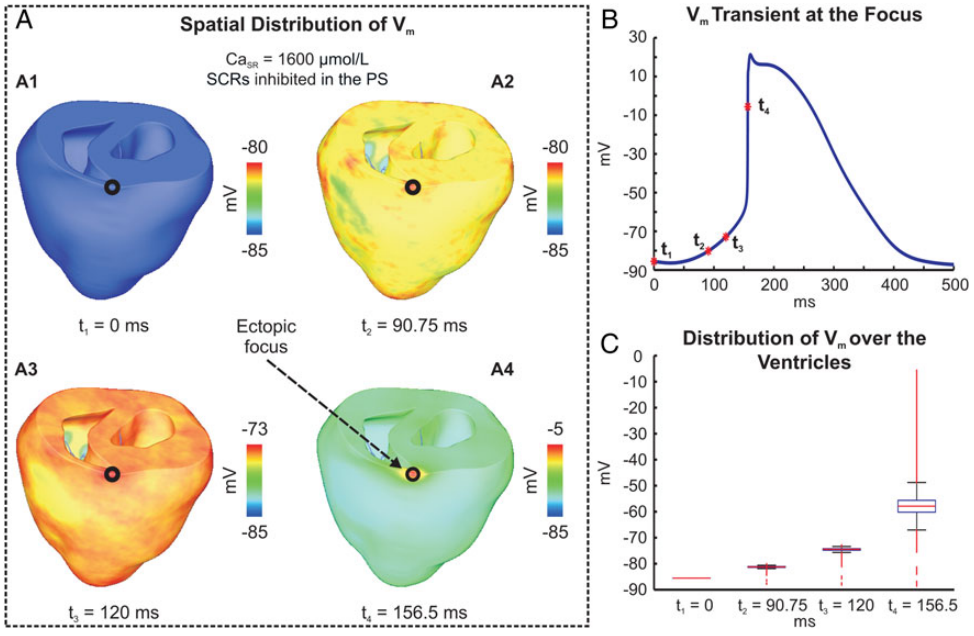

Figure 6 Genesis of a PVC in absence of SCRs in the PS. (*A*) Spatial distribution of V_m at time instants: t_1, t_{3-4} chosen as in *Figure 5*; $t_2 = 90.75$ ms when averaged $\Delta V_m = 5$ mV. (*B*) V_m trace at focal site. (*C*) Boxplots illustrating distribution of V_m over the ventricles at the time instants t_1 –t_4.

Results show that the sigmoid rise of p_{AP} is shifted towards higher Ca_{SR} and is markedly steeper in tissue relative to isolated myocytes. This gives rise to a narrow banded critical Ca_{SR} threshold where the regime in which no PVCs occur is separated from the high-probability regime by a minor difference in Ca_{SR} (50 µmol/L). This critical threshold depends on tissue dimensionality. In a 1D structure, such as a strand, p_{AP} is higher and T_{AP} is shorter than in higher dimensional tissue (Supplementary material online, *Figure S2*). As a consequence, the critical Ca_{SR} threshold is lower in the 1D PS network (1500 µmol/L) than in the 3D ventricular myocardium (1550 µmol/L) and therefore PVCs emerge, with overwhelming likelihood in the PS, with ~68% occurring within a distance of <1 mm from a PVJ. At slightly higher Ca_{SR} above

the critical threshold and with SCR inhibited in the PS, PVCs also originated in the ventricles mostly at sites of lower electrotonic load. These PVCs may emerge in the presence of the PS as well; however, they are masked by foci arising earlier in the PS due to the shorter average T_{AP} there. Overall, the high probability and reduced timing variability of SCR events at Ca_{SR} beyond the critical threshold lead to a global diastolic depolarization, which drives the ventricles and the PS gradually to the firing threshold. Under such depolarized conditions, no explicit synchronization mechanism is required for a cluster of cells to overcome source–sink mismatches.

4.1 Triggered activity in tissue

Experimental studies indicate that most ventricular tachycardias in non-ischaemic HF are initiated by non-reentrant focal mechanisms[9,10,26] such as SCR-triggered DADs. While underlying mechanisms are well understood in isolated myocytes, circumstances under which propagated APs are induced in the intact heart remain unclear. While APs are elicited in isolated myocytes once the membrane is depolarized above the threshold of I_{Na} activation, this is insufficient in tissue. According to the liminal length concept, the net ionic current generated by tissue around a focal site within the radius of electrotonic influence must become inward to initiate a propagated response.[27,28] Therefore, a DAD-triggered event may propagate only if sufficiently well synchronized SCR events occur in a large cluster of adjacent cells.[29] Moreover, due to electrotonic current flow via gap junctions, less current is available for local depolarization, requiring more I_{NCX} current for the same ΔV_m as in isolated myocytes. Even at an elevated Ca_{SR} of 1450 μmol/L which was associated with a p_{AP} of 100% in isolated myocytes, the average ΔV_m was markedly reduced in the 1D strand and p_{AP} was only 29%. No propagated APs were observed at $Ca_{SR} < 1450$ μmol/L in tissue, although intrinsic SCR metrics (total number of SCRs, T_{SCR} and ΔCa_s) remained unaffected by coupling (data not shown). Both average T_{SCR} and its variance were noticeably lowered at this Ca_{SR} (*Figure 2C*), but the temporal coincidence of SCR events was still insufficient to trigger a propagated AP. Thus, the combined effects of insufficient coincidence of SCR events and electrotonic loading led to a reduced ΔV_m, preventing the initiation of PVCs.

The role of electrotonic currents in suppressing ectopic excitations has been studied experimentally and computationally.[30–32] In a simulation study, Xie *et al.*[31] aimed to establish quantitatively the size of a cluster of cells needed to undergo a DAD in synchrony to initiate AP propagation. As expected on geometric grounds, the source–sink mismatch was most severe in 3D under normal coupling conditions, necessitating a large cluster of cells (~817 k cells) to fire. While this notion is compatible with our findings in that SCR events must occur in a large number of cells with a sufficiently close coincidence, our results suggest different conclusions regarding the underlying mechanism for spatial synchronization. This is mainly due to very different experimental conditions considered. Xie *et al.*[31] tested a scenario where all cells within a given region synchronously underwent a DAD, whereas outside the region, no DADs occurred. Under these conditions, a sharp gradient builds up between depolarizing cells within the region and cells at rest in the outside. This represents a limiting case of a source–sink relationship, which maximizes the electrotonic load imposed on a focal site. In the scenario considered in this study, timing and location of DADs were determined entirely by the stochastic nature of SCR events and by electrotonic loading. Under such conditions, it is extremely unlikely that a sharp gradient between a focal cluster and adjacent tissue builds up. Rather, our findings suggest that ectopic foci form in tissue only at sufficiently high Ca_{SR} at which p_{AP} is close to 100%. That is, essentially all cells undergo a SCR event and the variability in T_{SCR} is narrowed down to achieve a sufficient degree of coincidence (*Figure 2A* and *C*). This gives rise to a global depolarization that drives the tissue gradually to the firing threshold (see Supplementary material online, *Video S2*). As all cells slowly depolarize, to slightly different extents and with some jitter in timing, electrotonic currents smooth out this ripple, but the electrotonic load upon individual cells is minor. Thus fairly small clusters of cells, which are electrotonically favoured or undergo by chance a larger SCR event, are able to trigger a propagated AP. However, under realistic conditions, we expect tissue scale heterogeneities in both Ca^{2+} cycling properties and ion channels regulating the AP. Thus, we expect that focal excitations will occur in regions where the number of SCR events is largest and coordinated. Indeed, in line scan images of Ca^{2+} waves in a whole rat heart, Wasserstrom *et al.*[25] observed a PVC coinciding with the point when most of the cells within the experimental field undergo SCR or where ion channel conductances were such that an SCR event induced a larger ΔV_m, i.e. in regions of lower (higher) I_{K1} (I_{NCX}) conductance. Moreover, as shown by Xie *et al.*,[31] regional decreases in cellular coupling, as with reduced gap junction density or fibrosis, reduce conductivity, thereby lowering conduction velocity, and shorten space constant and liminal length. Under such conditions of reduced electrotonic load, the overall number of cells required to trigger a propagated response is much smaller, implicating a bias for PVCs to originate there. Indeed, Myles *et al.*[30] demonstrated that gap junction uncoupling increases the occurrence of PVCs in the intact rabbit heart. This is also supported by our own simulations (data not shown) in which intracellular conductivities were significantly reduced by a factor of 10. This led to a reduction in conduction velocity by 74 and 78% in longitudinal and transverse direction, respectively. Under these conditions, the calcium-membrane voltage coupling gain increased, and the Ca_{SR} threshold for PVC formation was reduced by 50 μmol/L. However, location and spatial scale of such regions of altered coupling or electrophysiological properties is highly non-trivial and is likely dependent on the precise details of the electrophysiological gradients and structural heterogeneities involved.

4.2 Role of the His-Purkinje network in PVC formation

Several studies have documented the greater vulnerability of the PS to PVCs than the ventricular myocardium.[10,26,33,34] Analysis of epicardial breakthrough patterns in ventricular tachycardia suggested ectopic focal sources in the His-Purkinje network.[10] Higher susceptibility of the PS to PVCs is attributed either to differences in cellular electrophysiology[34] or to tissue scale properties such as electrotonic load and liminal length.[35,36] A recent modelling study of Li and Rudy[34] provided evidence that in Purkinje cells, Ca_{SR} is higher and excitation threshold is lower due to the presence of the hyperpolarization-activated 'funny current' and a reduced I_{K1} current. This is corroborated by experimental findings showing that reduced I_{K1} is a key determinant for the greater calcium-membrane voltage coupling gain and genesis of PVCs in Purkinje fibres.[37] On the other hand, Cerrone *et al.*[10] used a simplified computer model of two thin tissue strips connected to a larger 2D sheet of tissue to mimic electrotonic loading conditions at PVJs. Their results support the notion that DADs are more likely to reach threshold within the thin fibres of the PS rather than in the 3D ventricular muscle due to the lower electrotonic load imposed on cells in the PS. This result is important as it demonstrates, for the first time, that

tissue geometry may play an important role in predisposing locations of lowered electrotonic load to the formation of PVCs.

In this study, a highly detailed computer model of rabbit ventricles and PS was employed to elucidate the influence of electrotonic load upon probability, location, and timing of PVCs. For this sake, any electrophysiological heterogeneity, which may be present in the rabbit heart *in vivo*, was ignored. Thus electrotonic load is the only tissue scale factor, which is subjected to spatial variation, any effects due to functional heterogeneities can be ruled out. PVCs of origin in the PS started to appear at a critical Ca_{SR} of 1500 μmol/L (*Figure 4A* and *C*). A further increase in Ca_{SR} did not entail a further increase in p_{AP}, nor did it change the overall distribution of focal sites, rather a further reduction in T_{AP} was observed. PVCs originated everywhere throughout the PS (*Figure 4B* and *C* and Supplementary material online, *Video S1*), but with a noticeable bias towards locations in the vicinity of PVJs, with about ∼68% of PVCs originating within a distance of <1 mm away from the closest PVJ. All sites, which fired more than once were in close proximity to a PVJ. This bias is explained by considering that the PVJ is modelled as a discrete resistive coupling between the terminal end of the PS and the ventricles. Coupling resistances, which were chosen to reproduce experimentally observed delays in anterograde and retrograde impulse transduction across the PVJ,[18] were high enough to lower the electrotonic load in the vicinity of the PVJs. Indeed, increasing the resistance across the junctions to further reduce the electrotonic load imposed by the ventricles upon the PS (data not shown) reinforced this trend. The number of foci increased from 68% within an average distance of ∼0.7 mm to 84% within an average distance of 0.2 mm from a PVJ (Ca_{SR} of 1600 μmol/L).

4.3 Triggered activity in ventricles

At a Ca_{SR} of 1500 μmol/L, PVCs originated, without exception, in the PS (*Figure 4A*). When SCRs were inhibited in the PS, no PVCs were observed. However, at a marginally higher $Ca_{SR} \geq 1550$ μmol/L, PVCs started to appear in the ventricles in all experiments (*Figure 4D*). PVC formation in this case is readily explained by the tissue-scale mechanisms elucidated earlier. SCR events occur virtually everywhere in the ventricles with sufficiently close coincidence such that the resulting inward currents summate to depolarize the resting potential gradually towards the firing threshold. PVCs tend to originate then in regions where the number of SCR events by chance is higher or where electrotonic load is lower. Indeed, almost all PVCs appeared along the tissue surface and tended to cluster along the edges of the ventricular base where electrotonic load is reduced.

While our results suggest that PVC formation at high Ca_{SR} is likely to occur in the ventricles, with an intact PS, PVCs always originated there first due to the shorter T_{AP} (*Figure 4C*). Overall, our results strongly support the notion that the one-dimensional PS is a very likely source of PVCs in the intact ventricles. Results summarized in *Figure 4* are compatible with findings reported by Cerrone *et al.*,[10] where optical maps of the endocardium in an episode of non-sustained multifocal tachycardia revealed that focal discharges at multiple locations were present, all of which were shown to originate within the PS. Our findings are further corroborated by simulations in simpler geometric models (Supplementary material online, *Figure S2*) which emphasize the high sensitivity of PVCs to dimensionality. With increasing dimensionality, probability of PVCs decreases while T_{AP} increases, thus indicating that PVCs appear not only with higher frequency, but also earlier in the 1D PS than in the 3D myocardium.

4.4 Steep sigmoid dependence of PVC probability upon Ca_{SR}

An important finding of this study is that the probability p_{AP} in tissue has a very steep sigmoid dependence on Ca_{SR} (*Figure 4A*). This result is surprising since p_{AP} in an isolated myocyte exhibits a much less steep dependence, suggesting that electrotonic coupling has a substantial effect on the shape of the p_{AP} curve. This result can be explained by the stochasticity of SCR in a population of cells in tissue, along with the effect of electrotonic coupling. As shown in a theoretical study, the mean T_{AP} is exponentially dependent on system parameters[22] and, as a consequence, the fraction of ectopic excitations observed within a finite duration pause following pacing will go from 0 to 1 over a small change in Ca_{SR} (see Supplementary material online for details).

4.5 SCRs and PVC formation in HF

In this study, key parameters of the MSH myocyte model were modified, in the context of HF remodelling, to increase its propensity for DADs. However, the failing heart undergoes a more complex set of electrophysiological changes, where altered Ca^{2+} cycling, AP prolongation, and gap junction remodelling are hallmark features favouring triggered activity arising from afterdepolarizations.[2,12,23,30] Abnormal RyR function is a key pathophysiological mechanism in HF. Experimental studies indicate that the SR content is reduced in HF.[12,38] Thus, it seems contradictory that SCR events due to Ca^{2+} overload play a significant role in PVC formation. However, unlike in this study where SCR events have a functional dependence on Ca_{SR}, in HF they have been attributed to an increased Ca^{2+} leak from the SR due to RyR phosphorylation.[38] In this scenario, the threshold level for SCRs is lowered and the amount of Ca_{SR} required to induce SCRs is reduced. Thus pharmacological strategies aiming to raise the threshold for SCRs in HF by stabilizing the RyRs may have potential benefits in PVC prevention. Indeed, Dantrolene has been demonstrated to preserve inotropy while inhibiting diastolic SCRs but not systolic releases in HF cells.[39]

4.6 Study limitations

While the computer model used in this study is state-of-the-art with regard to the representation of biventricular anatomy, topology of the PS network, modelling of PVJs and multiscale representation of stochastic aspects of Ca^{2+} cycling, it is simplistic in other aspects. First, although a Ca-binding site on the luminal side of the RyR channel is believed to play a role in SCR, only a functional dependence on Ca_{SR} is considered in our phenomenological Ca^{2+} model. However, a luminal sensor would only pose additional sensitivity to the gradient of Ca^{2+} across the SR membrane making SCRs even more sensitive to Ca_{SR}. Secondly, the cell model was modified to represent some key electrophysiological changes observed under HF conditions, namely up- and down-regulation of I_{NCX} and I_{K1}, respectively. The rationale behind this choice is that DAD-triggered activity, the focus of this study, is extremely sensitive to the ratio of inward to outward currents near the threshold for an AP with I_{NCX} and I_{K1} being the two main factors. Investigating how PVC formation is affected by other remodelling process, such as AP prolongation, enhanced heterogeneity or conduction slowing, would require numerous adjustments, which would be a study in its own right. Finally, all known spatial heterogeneities in cellular electrophysiology have been fully ignored. This deliberate choice in the design of this *in-silico* model allowed us to dissect out the role of the main tissue-scale parameter of interest of this study—the influence of electrotonic load. By using the exact same cellular makeup for both

ventricles and PS, any influence of functional heterogeneities can be ruled out.

5. Conclusion

Using an anatomically accurate computer model of rabbit ventricles and His-Purkinje system this study found that the probability of SCR-mediated ectopic excitations in tissue increases dramatically due to small changes in Ca_{SR}. This high sensitivity is observed close to a critical Ca_{SR} above which p_{AP} increases rapidly, from 0 to 100%. The 0 and 100% probability regime is separated by a very narrow corridor of Ca_{SR} of only ~3.3%. This critical threshold is due to the influence of electrotonic load on the probabilistic nature of SCR. As a consequence, in the ventricles there is a range of Ca_{SR} where PVCs occur exclusively in the PS, mostly in the immediate vicinity of a PVJ. While PVCs may also occur in the 3D myocardium at higher Ca_{SR}, due to longer T_{AP}, these are masked by ectopic excitations occurring earlier in the PS, suggesting the PS as the lone source of PVCs. The strong sensitivity of ectopic excitations on Ca_{SR} suggests that therapeutic approaches that target this relationship can be highly effective to prevent PVCs.

Supplementary material

Supplementary material is available at *Cardiovascular Research* online.

Acknowledgements

The authors gratefully acknowledge the valuable suggestions of Dr Simon Sedej, Dr Brigitte Pelzmann, and Dr Klaus Zorn-Pauly in reading the manuscript.

Conflict of interest: none declared.

Funding

This work was supported by the National Institutes of Health (grant number 1RO1 HL 10119601) and by the Austrian Science Fund (grant number F3210-N18).

References

1. Mehta D, Curwin J, Gomes JA, Fuster V. Sudden death in coronary artery disease: acute ischemia versus myocardial substrate. *Circulation* 1997;**96**:3215–3223.
2. Tomaselli GF, Beuckelmann DJ, Calkins HG, Berger RD, Kessler PD, Lawrence JH, Kass D, Feldman AM, Marban E. Sudden cardiac death in heart failure. The role of abnormal repolarization. *Circulation* 1994;**90**:2534–2539.
3. Zimetbaum P, Josephson ME. Evaluation of patients with palpitations. *N Engl J Med* 1998;**338**:1369–1373.
4. Zhang S, Skinner JL, Sims AL, Rollins DL, Walcott GP, Smith WM, Ideker RE. Three-dimensional mapping of spontaneous ventricular arrhythmias in a canine thrombotic coronary occlusion model. *J Cardiovasc Electrophysiol* 2000;**11**:762–772.
5. Nuyens D, Stengl M, Dugarmaa S, Rossenbacker T, Compernolle V, Rudy Y, Smits JF, Flameng W, Clancy CE, Moons L, Vos MA, Dewerchin M, Benndorf K, Collen D, Carmeliet E, Carmeliet P. Abrupt rate accelerations or premature beats cause life-threatening arrhythmias in mice with long-QT3 syndrome. *Nat Med* 2001;**7**:1021–1027.
6. Capogrossi MC, Houser SR, Bahinski A, Lakatta EG. Synchronous occurrence of spontaneous localized calcium release from the sarcoplasmic reticulum generates action potentials in rat cardiac ventricular myocytes at normal resting membrane potential. *Circ Res* 1987;**61**:498–503.
7. Schlotthauer K, Bers DM. Sarcoplasmic reticulum Ca2+ release causes myocyte depolarization: underlying mechanism and threshold for triggered action potentials. *Circ Res* 2000;**87**:774–780.
8. Boyden PA, Pu J, Pinto J, Keurs HE. Ca(2+) transients and Ca(2+) waves in purkinje cells: role in action potential initiation. *Circ Res* 2000;**86**:448–455.
9. Pogwizd SM. Nonreentrant mechanism underlying spontaneous ventricular arrhythmias in a model of nonischemic heart failure in rabbits. *Circulation* 1995;**92**:1034–1048.
10. Cerrone M, Noujaim SF, Tolkacheva EG, Talkachou A, O'Connell R, Berenfeld O, Anumonwo J, Pandit SV, Vikstrom K, Napolitano C, Priori SG, Jalife J. Arrhythmogenic mechanisms in a mouse model of catecholaminergic polymorphic ventricular tachycardia. *Circ Res* 2007;**101**:1039–1048.
11. Bai Y, Jones PP, Guo J, Zhong X, Clark RB, Zhou Q, Wang R, Vallmitjana A, Benitez R, Hove-Madsen L, Semeniuk L, Guo A, Song LS, Duff HJ, Chen SR. Phospholamban knockout breaks arrhythmogenic Ca2+ waves and suppresses catecholaminergic polymorphic ventricular tachycardia in mice. *Circ Res* 2013;**113**:517–526.
12. Sipido KR. Calcium overload, spontaneous calcium release, and ventricular arrhythmias. *Heart Rhythm* 2006;**3**:977–979.
13. Kass RS, Lederer WJ, Tsien RW, Weingart R. Role of calcium ions in transient inward currents and aftercontractions induced by strophanthidin in cardiac Purkinje fibers. *J Physiol (Lond)* 1978;**281**:187–208.
14. Sipido KR, Volders PG, de Groot SH, Verdonck F, Van de Werf F, Wellens HJ, Vos MA. Enhanced Ca(2+) release and Na/Ca exchange activity in hypertrophied canine ventricular myocytes: potential link between contractile adaptation and arrhythmogenesis. *Circulation* 2000;**102**:2137–2144.
15. Vassalle M, Lin CI. Calcium overload and cardiac function. *J Biomed Sci* 2004;**11**:542–565.
16. Chen W, Aistrup G, Wasserstrom JA, Shiferaw Y. A mathematical model of spontaneous calcium release in cardiac myocytes. *Am J Physiol Heart Circ Physiol* 2011;**300**:H1794–H1805.
17. Mahajan A, Shiferaw Y, Sato D, Baher A, Olcese R, Xie LH, Yang MJ, Chen PS, Restrepo JG, Karma A, Garfinkel A, Qu Z, Weiss JN. A rabbit ventricular action potential model replicating cardiac dynamics at rapid heart rates. *Biophys J* 2008;**94**:392–410.
18. Boyle PM, Deo M, Plank G, Vigmond EJ. Purkinje-mediated effects in the response of quiescent ventricles to defibrillation shocks. *Ann Biomed Eng* 2010;**38**:456–468.
19. Restrepo JG, Karma A. Spatiotemporal intracellular calcium dynamics during cardiac alternans. *Chaos* 2009;**19**:037115.
20. Rovetti R, Cui X, Garfinkel A, Weiss JN, Qu Z. Spark-induced sparks as a mechanism of intracellular calcium alternans in cardiac myocytes. *Circ Res* 2010;**106**:1582–1591.
21. Gaur N, Rudy Y. Multiscale modeling of calcium cycling in cardiac ventricular myocyte: macroscopic consequences of microscopic dyadic function. *Biophys J* 2011;**100**:2904–2912.
22. Chen W, Asfaw M, Shiferaw Y. The statistics of calcium-mediated focal excitations on a one-dimensional cable. *Biophys J* 2012;**102**:461–471.
23. Pogwizd SM, Schlotthauer K, Li L, Yuan W, Bers DM. Arrhythmogenesis and contractile dysfunction in heart failure: roles of sodium-calcium exchange, inward rectifier potassium current, and residual beta-adrenergic responsiveness. *Circ Res* 2001;**88**:1159–1167.
24. Vigmond EJ, Hughes M, Plank G, Leon LJ. Computational tools for modeling electrical activity in cardiac tissue. *J Electrocardiol*. 2003;**36**(suppl.):69–74.
25. Wasserstrom JA, Shiferaw Y, Chen W, Ramakrishna S, Patel H, Kelly JE, O'Toole MJ, Pappas A, Chirayil N, Bassi N, Akintilo L, Wu M, Arora R, Aistrup GL. Variability in timing of spontaneous calcium release in the intact rat heart is determined by the time course of sarcoplasmic reticulum calcium load. *Circ Res* 2010;**107**:1117–1126.
26. Rushton WAH. Initiation of the propagated disturbance. *Proc R Soc B* 1937;**124**:210–243.
27. Joyner RW, Wang YG, Wilders R, Golod DA, Wagner MB, Kumar R, Goolsby WN. A spontaneously active focus drives a model atrial sheet more easily than a model ventricular sheet. *Am J Physiol Heart Circ Physiol* 2000;**279**:H752–H763.
28. Houser SR. When does spontaneous sarcoplasmic reticulum Ca(2+) release cause a triggered arrhythmia? Cellular versus tissue requirements. *Circ Res* 2000; **87**:725–727.
29. Joyner RW, Sugiura H, Tan RC. Unidirectional block between isolated rabbit ventricular cells coupled by a variable resistance. *Biophys J* 1991;**60**:1038–1045.
30. Myles RC, Wang L, Kang C, Bers DM, Ripplinger CM. Local β-adrenergic stimulation overcomes source-sink mismatch to generate focal arrhythmia. *Circ Res* 2012;**110**:1454–1464.
31. Xie Y, Sato D, Garfinkel A, Qu Z, Weiss JN. So little source, so much sink: requirements for afterdepolarizations to propagate in tissue. *Biophys J* 2010;**99**:1408–1415.
32. Liu N, Colombi B, Memmi M, Zissimopoulos S, Rizzi N, Negri S, Imbriani M, Napolitano C, Lai FA, Priori SG. Arrhythmogenesis in catecholaminergic polymorphic ventricular tachycardia: insights from a RyR2 R4496C knock-in mouse model. *Circ Res* 2006;**99**:292–298.
33. Deo M, Boyle PM, Kim AM, Vigmond EJ. Arrhythmogenesis by single ectopic beats originating in the Purkinje system. *Am J Physiol Heart Circ Physiol* 2010;**299**:H1002–H1011.
34. Li P, Rudy Y. A model of canine purkinje cell electrophysiology and Ca(2+) cycling: rate dependence, triggered activity, and comparison to ventricular myocytes. *Circ Res* 2011;**109**:71–79.
35. Fozzard HA, Schoenberg M. Strength-duration curves in cardiac Purkinje fibres: effects of liminal length and charge distribution. *J Physiol* 1972;**226**:593–618.
36. Lindemans FW, Denier Van der Gon JJ. Current thresholds and liminal size in excitation of heart muscle. *Cardiovasc Res* 1978;**12**:477–485.
37. Maruyama M, Joung B, Tang L, Shinohara T, On YK, Han S, Choi EK, Kim DH, Shen MJ, Weiss JN, Lin SF, Chen PS. Diastolic intracellular calcium-membrane voltage coupling gain and postshock arrhythmias: role of purkinje fibers and triggered activity. *Circ Res* 2010;**106**:399–408.
38. Belevych AE, Radwański PB, Carnes CA, Györke S. 'Ryanopathy': causes and manifestations of RyR2 dysfunction in heart failure. *Cardiovasc Res* 2013;**98**:240–247.
39. Maxwell JT, Domeier TL, Blatter LA. Dantrolene prevents arrhythmogenic Ca2+ release in heart failure. *Am J Physiol Heart Circ Physiol* 2012;**302**:H953–H963.